The Astrophysical Journal Supplement Series, 176:424–437, 2008 June

THE *HUBBLE SPACE TELESCOPE* ADVANCED CAMERA FOR SURVEYS COMA CLUSTER SURVEY. I. SURVEY OBJECTIVES AND DESIGN[1]

David Carter,[2] Paul Goudfrooij,[3] Bahram Mobasher,[3] Henry C. Ferguson,[3] Thomas H. Puzia,[4] Alfonso L. Aguerri,[5] Marc Balcells,[5] Dan Batcheldor,[6] Terry J. Bridges,[7] Jonathan I. Davies,[8] Peter Erwin,[9,10] Alister W. Graham,[11] Rafael Guzmán,[12] Derek Hammer,[13] Ann Hornschemeier,[14] Carlos Hoyos,[12,15] Michael J. Hudson,[16] Avon Huxor,[17] Shardha Jogee,[18] Yutaka Komiyama,[19] Jennifer Lotz,[20] John R. Lucey,[21] Ronald O. Marzke,[22] David Merritt,[6] Bryan W. Miller,[23] Neal A. Miller,[13,24] Mustapha Mouhcine,[2] Sadanori Okamura,[25] Reynier F. Peletier,[26] Steven Phillipps,[17] Bianca M. Poggianti,[27] Ray M. Sharples,[21] Russell J. Smith,[21] Neil Trentham,[28] R. Brent Tully,[29] Edwin Valentijn,[26] and Gijs Verdoes Kleijn[26]

Received 2007 September 1; accepted 2008 January 21

ABSTRACT

We describe the *HST* ACS Coma Cluster Treasury survey, a deep two-passband imaging survey of one of the nearest rich clusters of galaxies, the Coma Cluster (Abell 1656). The survey was designed to cover an area of 740 arcmin^2 in regions of different density of both galaxies and intergalactic medium within the cluster. The ACS failure of 2007 January 27 leaves the survey 28% complete, with 21 ACS pointings (230 arcmin^2) complete, and partial data for a further four pointings (44 arcmin^2). The predicted survey depth for 10 σ detections for optimal photometry of point sources is $g' = 27.6$ in the F475W filter and $I_C = 26.8$ mag in F814 (AB magnitudes). Initial simulations with artificially injected point sources show 90% recovered at magnitude limits of $g' = 27.55$ and $I_C = 26.65$. For extended sources, the predicted 10 σ limits for a 1 arcsec^2 region are $g' = 25.8$ mag arcsec^{-2} and $I_C = 25.0$ mag arcsec^{-2}. We highlight several motivating science goals of the survey, including study of the faint end of the cluster galaxy luminosity function, structural parameters of dwarf galaxies, stellar populations and their effect on colors and color gradients, evolution of morphological components in a dense environment, the nature of ultracompact dwarf galaxies, and globular cluster populations of cluster galaxies of a range of luminosities and types. This survey will also provide a local rich cluster benchmark for various well-known *global* scaling relations and explore new relations pertaining to the *nuclear* properties of galaxies.

Subject headings: galaxies: clusters: individual (Abell 1656) — galaxies: fundamental parameters — galaxies: luminosity function, mass function — galaxies: photometry — galaxies: stellar content — galaxies: structure

[1] Based on observations with the NASA/ESA *Hubble Space Telescope* obtained at the Space Telescope Science Institute, which is operated by the association of Universities for Research in Astronomy, Inc., under NASA contract NAS5-26555. These observations are associated with program GO10861.

[2] Astrophysics Research Institute, Liverpool John Moores University, Twelve Quays House, Egerton Wharf, Birkenhead CH41 1LD, UK.
[3] Space Telescope Science Institute, 3700 San Martin Drive, Baltimore, MD 21218.
[4] Dominion Astrophysical Observatory, Herzberg Institute of Astrophysics, National Research Council of Canada, 5071 West Saanich Road, Victoria, BC V9E 2E7, Canada.
[5] Instituto de Astrofísica de Canarias, C/Vía Lactea s/n, 38200 La Laguna, Tenerife, Spain.
[6] Department of Physics, Rochester Institute of Technology, 85 Lomb Memorial Drive, Rochester, NY 14623.
[7] Department of Physics, Engineering Physics and Astronomy, Queen's University, Kingston, ON K7L 3N6, Canada.
[8] School of Physics and Astronomy, Cardiff University, The Parade, Cardiff CF24 3YB, UK.
[9] Max-Planck-Institut für Extraterrestrische Physik, Giessenbachstrasse, D-85748 Garching, Germany.
[10] Universitäts-Sternwarte München, Scheinerstrasse 1, D-81679 München, Germany.
[11] Centre for Astrophysics and Supercomputing, Swinburne University of Technology, Hawthorn, VIC 3122, Australia.
[12] Department of Astronomy, University of Florida, P.O. Box 112055, Gainesville, FL 32611.
[13] Department of Physics and Astronomy, Johns Hopkins University, 3400 North Charles Street, Baltimore, MD 21218.
[14] Laboratory for X-Ray Astrophysics, NASA Goddard Space Flight Center, Code 662.0, Greenbelt, MD 20771.
[15] Departamento de Física Teórica, Universidad Autónoma de Madrid, Carretera de Colmenar Viejo km 15.600, 28049 Madrid, Spain.
[16] Department of Physics and Astronomy, University of Waterloo, 200 University Avenue West, Waterloo, ON N2L 3G1, Canada.
[17] Astrophysics Group, H. H. Wills Physics Laboratory, University of Bristol, Tyndall Avenue, Bristol BS8 1TL, UK.
[18] Department of Astronomy, University of Texas at Austin, 1 University Station C1400, Austin, TX 78712.
[19] Subaru Telescope, National Astronomical Observatory of Japan, 650 North A'ohoku Place, Hilo, HI 96720.
[20] Leo Goldberg Fellow, National Optical Astronomy Observatory, 950 North Cherry Avenue, Tucson, AZ 85719.
[21] Department of Physics, University of Durham, South Road, Durham DH1 3LE, UK.
[22] Department of Physics and Astronomy, San Francisco State University, San Francisco, CA 94132-4163.
[23] Gemini Observatory, Casilla 603, La Serena, Chile.
[24] Jansky Fellow of the National Radio Astronomy Observatory. The National Radio Astronomy Observatory is a facility of the National Science Foundation operated under cooperative agreement by Associated Universities, Inc.
[25] Department of Astronomy, University of Tokyo, 7-3-1 Hongo, Bunkyo, Tokyo 113-0033, Japan.
[26] Kapteyn Astronomical Institute, University of Groningen, P.O. Box 800, 9700 AV Groningen, The Netherlands.
[27] INAF-Osservatorio Astronomico di Padova, Vicolo dell'Osservatorio 5, Padova I-35122, Italy.
[28] Institute of Astronomy, Madingley Road, Cambridge CB3 0HA, UK.
[29] Institute for Astronomy, University of Hawaii, 2680 Woodlawn Drive, Honolulu, HI 96822.

1. INTRODUCTION AND BACKGROUND

The Coma Cluster of galaxies, Abell 1656, is along with the Perseus Cluster the nearest rich and dense cluster environment. Unlike the Perseus Cluster, it is at high Galactic latitude ($b = 87.9^\circ$), and it has been a popular target for study at all wavelengths. Progressively deeper wide-area photometric surveys of Coma have become available over the past 30 years, and wave band coverage has spread from the original *B*- and *V*-band surveys into the near-ultraviolet and infrared (Godwin & Peach 1977; Godwin et al. 1983 [GMP]; Komiyama et al. 2002; Adami et al. 2006; Eisenhardt et al. 2007). A larger area around Coma is covered by the imaging part of Data Release 5 of the Sloan Digital Sky Survey (SDSS; Adelman-McCarthy et al. 2007). From these surveys, samples of galaxies have been selected for spectroscopic study, which has resulted in an understanding of the internal dynamics of the cluster (Colless & Dunn 1996; Mobasher et al. 2001; Edwards et al. 2002; Gutiérrez et al. 2004), the internal dynamics of cluster members (Lucey et al. 1991; Jorgensen et al. 1996; Smith et al. 2004; Matković & Guzmán 2005; Cody et al. 2007), and their mean luminosity-weighted stellar ages, abundances, and α-enhancement (Bower et al. 1992a, 1992b; Guzmán et al. 1992; Caldwell et al. 1993; Jorgensen 1999; Poggianti et al. 2001; Moore et al. 2002; Nelan et al. 2005; Smith et al. 2006; Matković et al. 2007). Coma presents us with the best opportunity to study large samples of galaxies of different luminosity, environment, and morphological type, but at a common distance and with a common Galactic extinction.

There is good agreement on the distance to the Coma Cluster, with independent studies using six different methods yielding values in the range 84–108 Mpc, as summarized in Table 1. These values fit well with the current concordance cosmology: assuming $H_0 = 71$ km s^{-1} Mpc^{-1}, $\Omega_\lambda = 0.73$, $\Omega_m = 0.27$, and a redshift $z = 0.0231$ gives a distance of 99.3 Mpc. In this paper we assume a distance of 100 Mpc, equivalent to a distance modulus of 35.00.

Coma lies in a rich region of the large-scale distribution of galaxies, at the intersection of a number of filaments. Figure 1 shows two projections of the distribution of galaxies in supergalactic coordinates in the region of Coma and the nearby richness class 2 cluster Abell 1367. The Great Wall (Geller & Huchra 1989), a vertical structure in the two panels of Figure 1, runs through these two clusters; other filaments intersect the Great Wall at the Coma Cluster.

There is a uniquely rich multiwavelength data set on the Coma Cluster. X-ray observations covering a large area of the cluster have been made with *ROSAT* (White et al. 1993) and *XMM-Newton* (Briel et al. 2001), showing the distribution and properties of the hot intracluster medium (ICM), and X-ray properties of individual galaxies have been studied by Finoguenov et al. (2004) and by Hornschemeier et al. (2006). Coma has been shown by the gamma-ray satellite *INTEGRAL* to be an extended hard X-ray/soft γ-ray source (Renaud et al. 2006). At soft X-ray and extreme-ultraviolet wavelengths there is a thermal excess (Lieu et al. 1996; Kaastra et al. 2003; Bonamente et al. 2003; Bowyer et al. 2004). *GALEX* has been used to observe the cluster in the mid- and near-ultraviolet and has sufficient spatial resolution to measure the UV properties of individual galaxies. In the infrared, studies of the galaxies have been made using *Spitzer*, both with IRAC at 3.6–8 μm (Jenkins et al. 2007) and with MIPS at 24 and 70 μm (Bai et al. 2006). At radio wavelengths, Very Large Array (VLA) continuum maps cover much of the cluster (N. Miller et al., in preparation), and in the H I 21 cm line there are extensive VLA imaging surveys (Bravo-Alfaro et al. 2000, 2001), and single-dish spectra and fluxes for samples of spiral galaxies (Gavazzi et al. 2006; Vogt et al. 2004).

This wealth of existing data makes Coma a prime target for studies of the origin and evolution of the galaxy content of clusters and of its interaction with the other components (gas and dark matter). Moreover, as the richest and best-studied local cluster, Coma is the zero-redshift baseline for many studies of high-redshift clusters (e.g., Jorgensen et al. 2006). Comparison between low- and high-redshift clusters is vital for our understanding of their evolution, which in turn is essential if we are to disentangle evolutionary effects from the properties that tell us about their formation.

We describe here the *Hubble Space Telescope* Advanced Camera for Surveys (*HST* ACS) Coma Cluster Treasury survey, which aims to provide an unparalleled database of high spatial resolution images of a sample of cluster galaxies. At the distance of the Coma Cluster ($\sim$100 Mpc), the resolution of *HST* ACS ($0.1''$) corresponds to $\sim$50 pc. This gives essentially the same physical resolution as ground-based observations have in Virgo and Fornax. Thus, the *HST* ACS Coma database provides a valuable comparison between high- and low-density clusters, for studies of the effect of environment on galaxy components.

While the *HST* observations are the prime data on which this survey is based, it has already generated numerous ancillary observations with facilities such as Subaru, Keck, MMT, and UKIRT. It is concurrent with surveys of the cluster in other wave bands, including the ultraviolet (*GALEX*), infrared (*Spitzer*), X-ray (*Chandra* and *XMM-Newton*), and radio (VLA).

2. SCIENTIFIC MOTIVATION

2.1. *The Luminosity Function*

The logarithmic slope of the low-mass end of the cold dark matter (ΛCDM) mass function has a slope $\alpha \approx -1.8$ (e.g., Somerville & Primack 1999). In contrast, the faint end of the field galaxy luminosity function (LF) has a slope $\alpha \approx -1.3$, when measured either from optically selected surveys (Blanton et al. 2005) or H I (Zwaan et al. 2005), or $\alpha \approx -1.0$, when measured in the *K* band (Gardner et al. 1997; Kochanek et al. 2001). Luminosity functions in clusters and groups are often not well fit by a single Schechter function (Smith et al. 1997) and are better modeled by a combination of a Gaussian and a Schechter function (Ferguson & Sandage 1991). The composite behavior of the LF and the trends with cluster richness are beginning to be understood in the context of the conditional LF (Cooray & Cen 2005), which provides a powerful conceptual framework for exploring the physics of galaxy formation via studies of halos (clusters and groups) of different mass. The suppression of the faint-end slope of the LF relative to the CDM mass function is widely believed to be due to photoionization by the metagalactic UV background, which suppresses star formation in low-mass halos. This predicts an environmental dependence (Tully et al. 2002) because the fraction of dwarf-mass subhalos that collapse before reionization is larger in higher mass halos, i.e., much larger in a 10^{14} $M_\odot$ halo than in a 10^{11} $M_\odot$ halo. This prediction can be tested directly with our survey, as the very faint end of the LF slope in Coma should be closer to the CDM prediction, and at least some of the dwarfs should have very old stellar populations.

From earlier *HST* WFPC2 data of a small area around NGC 4874 in the core of the Coma Cluster, Milne et al. (2007) determine a steep faint-end slope ($\alpha \approx -2.0$), which agrees with the slope for the faintest objects in a small-area imaging study by Bernstein et al. (1995) but not with studies using spectroscopic redshifts (Mobasher et al. 2003).

TABLE 1
THE DISTANCE TO COMA DETERMINED BY DIFFERENT TECHNIQUES

Technique	Distance (Mpc)	Distance Modulus	Reference
I-band Tully-Fisher	86.3 ± 6	34.68 ± 0.15	Tully & Pierce (2000)
K′-band SBF	85 ± 10	34.64 ± 0.27	Jensen et al. (1999)
I-band SBF	102 ± 14	35.04 ± 0.32	Thomsen et al. (1997)
D_n-σ	96 ± 6	34.90 ± 0.14	Gregg (1997)
Fundamental plane	108 ± 12	35.16 ± 0.25	Hjorth & Tanvir (1997)
Globular cluster LF	102 ± 6	35.05 ± 0.12	Kavelaars et al. (2000)

Measurements of the faint-end LF slope in the Virgo Cluster have been made by a number of authors, e.g., Trentham & Hodgkin (2002) and Sabatini et al. (2007). Trentham & Hodgkin (2002) find that the LF rises rapidly ($\alpha \approx -1.6$) between $M_B = -16$ and -14 but flattens faintward of this. The results of Sabatini et al. (2007) again suggest a steep slope between $M_B = -16$ and -14, flatter between $M_B = -14$ and -11. Trentham & Tully (2002) analyze the slope of the faint end of the LF in a number of lower density groups. They find a mean slope of $\alpha \approx -1.2$ over a large range from $M_B = -18$ to -10. Mieske et al. (2007) use surface brightness fluctuation (SBF) measurements to determine cluster membership in Fornax and find an even flatter faint-end slope, similar to that in the Local Group ($\alpha \approx -1.1$). These authors point out, however, that the absolute number of dwarfs per unit virial mass is higher in the lower density environments. Sabatini et al. (2007) concur that the luminosity function slope in the field is flatter than in the Virgo Cluster, although they parameterize this in terms of a dwarf-to-giant ratio (DGR). These studies present a consistent picture of a faint-end LF slope that is strongly dependent on the density of the environment, and our study of the Coma LF, at a variety of galaxy densities, will present an important extension to this work.

The area of the survey reduces the vulnerability of determinations of the faint-end slope to poor statistics and cosmic variance (Driver et al. 1998) and provides a sufficient range of galaxy density to test variations in the faint-end LF across different cluster environments (e.g., Phillipps et al. 1998). The depth and spatial resolution allow the use of surface brightness and morphological criteria to assess the probability of cluster membership (Trentham et al. 2001; Trentham & Tully 2002) and examination of the relative contribution of dE, dS0, and dIrr galaxies to the faint-end LF, and of the possible evolutionary

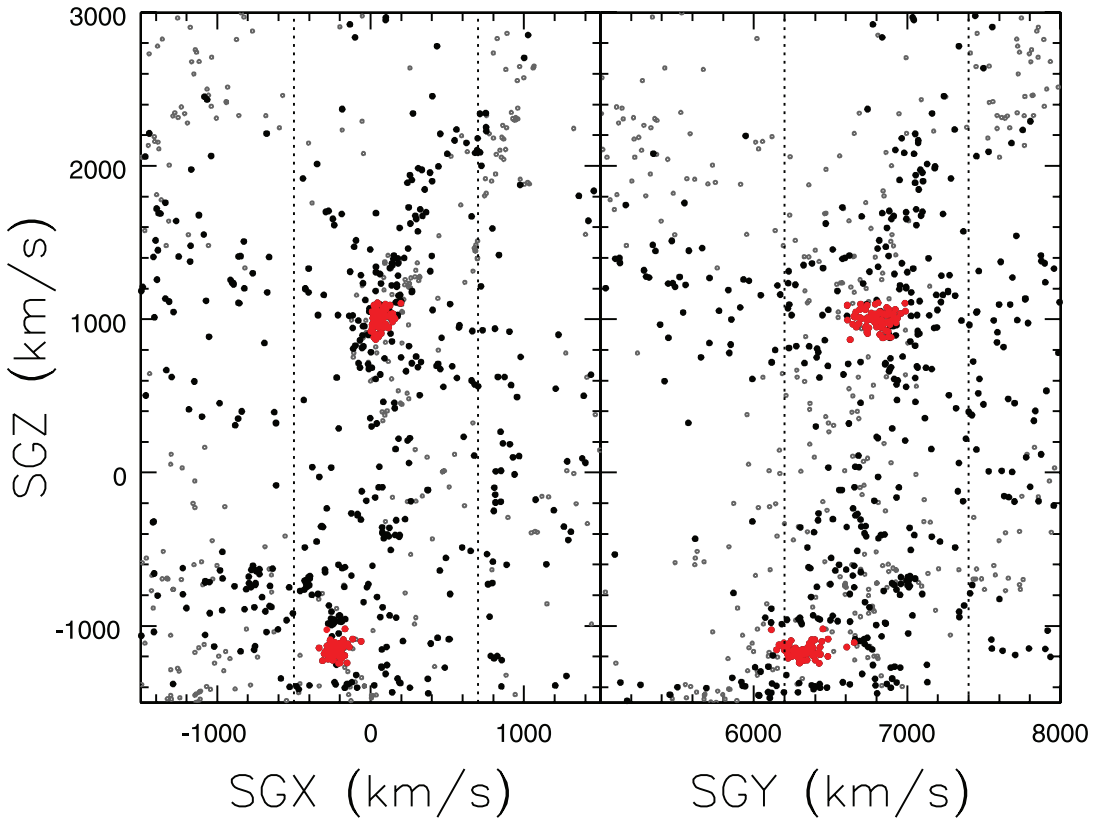

FIG. 1.—Location and environment of the Coma Cluster in supergalactic coordinates. *Left:* Projection onto supergalactic *Y*, close to the plane of the sky. *Right:* Projection onto supergalactic *X*; in this panel the horizontal (*Y*) axis is close to measured redshift. All axes are in equivalent *cz*. Positions of the points are derived from measured sky positions and redshifts. Members of Coma (*center*) and Abell 1367 (*bottom*) are plotted as filled red circles; for these galaxies the redshift used to compute the distance is the cluster redshift, with a random velocity offset chosen to make the cluster appear round. For non–cluster members, measured *cz* is used, and the positions are plotted as filled black circles if they have velocities within ±600 km s^{-1} of the Coma mean in the depth dimension in that particular panel and as open gray circles otherwise. The Great Wall is the structure at SG $Y \sim 6800$ km s^{-1} in the right panel and is seen face-on in the left panel

relationship between these types (Aguerri et al. 2005; Mastropietro et al. 2005).

Different formation mechanisms give rise to the disk, bulge, and bar components of galaxies. To understand the relative dominance of these physical processes in the universe therefore requires one to construct not simply a galaxy luminosity function, but separate bulge, bar, and disk luminosity functions (Driver et al. 2007a; Laurikainen et al. 2005). The dust-corrected Millenium Galaxy Catalogue (Driver et al. 2007b) provides a field galaxy comparison for the Coma component luminosity functions.

2.2. *Structure and Scaling Laws of Dwarf Galaxies*

Early-type galaxies exhibit well-defined empirical correlations between global galaxy parameters, such as luminosity, radius, surface brightness, color, velocity dispersion, and line strength indices (Kormendy 1985; Faber & Jackson 1976; Bender et al. 1992; Guzmán et al. 1993; Graham & Guzmán 2003). These scaling laws can tell us a great deal about the physical processes operating during galaxy formation, of which major contributors are star formation feedback (Efstathiou 2000), tidal interactions (Duc et al. 2004), and interactions with the hot intergalactic medium (Babul & Rees 1992; Roberts et al. 2004; Tully et al. 2002).

Despite being the most numerous galaxy type in nearby clusters, dE/dS0 galaxies are among the most poorly studied due to their low surface brightness (21 mag arcsec$^{-2} < \mu_e <$ 25 mag arcsec^{-2}). The scaling laws for dwarf ($M_V > -19$) elliptical galaxies are somewhat controversial; it is unclear whether dwarfs form a family of galaxies distinct from giants (Wirth & Gallagher 1984; Kormendy 1985; Caon et al. 1993) or a continuous sequence with them (Caldwell 1983; Graham & Guzmán 2003; Coté et al. 2007). The ACS survey will allow sophisticated parameterization of the surface brightness profiles of galaxies to $V \sim 21$ ($M_V \sim -14$) and measurement of basic structural parameters such as half-light radius and Sérsic (1968) index to $V \sim 23$ ($M_V \sim -12$). Such limits are similar to those for measuring velocity dispersions and line strengths with large ground-based telescopes. Substantial samples from multiobject spectrographs on 4 m class telescopes down to $B \sim 19$ already exist (see § 1).

The study of the scaling laws in various environments also provides the key observational reference needed to test specific predictions of current theoretical models of dwarf galaxy formation and evolution. For instance, the galaxy harassment model predicts that dE/dS0's in the highest density cluster regions should have steeper logarithmic light profiles, the fraction of nucleated dE/dS0's should be higher, the fraction of any remaining disk structure should be lower, and they should have higher metallicities than those located in lower density cluster environments (Moore et al. 1998).

2.3. *The Effect of Environment on Morphological Components*

The high density in the Coma Cluster core makes it an ideal place to investigate the morphology-density relation, in which the average bulge-to-disk (B/D) luminosity ratio increases with galaxy density (Dressler 1980). This is understood to result from transformation of spirals into early types through processes such as harassment (Moore et al. 1996) and the removal of dusty gas (Driver et al. 2008). An example of this transformation in progress may be the Coma Cluster galaxy GMP 3629 (Graham et al. 2003b). Furthermore, there is a strong cluster radial gradient in H I content in the spirals, those in the cluster core being severely depleted (Bothun et al. 1984; Bravo-Alfaro et al. 2000). This, together with similar results in Virgo, supports the notion of gas stripping and the subsequent cessation of star formation (Conselice et al. 2003). From a quantitative morphological analysis using high-quality ground-based images, Gutiérrez et al. (2004) find that disks in the Coma core are 30% smaller than in the field for a given bulge size.

Bulge-disk decomposition in the presence of nuclear components depends critically on spatial resolution (Balcells et al. 2003). The high resolution of ACS allows identification of disks, unobscured primary and nuclear bars, classical bulges, resonance starburst rings, compact disks, disky bulges, and pseudobulges (e.g., Kormendy & Kennicutt 2004; Athanassoula 2005). While observations in the rest-frame I band (F814W) may miss some highly obscured morphological features, a comparison of the optical properties across field and dense clusters will set important constraints on how environment influences the morphology and structure of galaxies. The radial dependence of bulge and disk morphologies can constrain the roles of mergers (Aguerri et al. 2001) and of disk truncation processes.

2.3.1. *Stellar Bars and Disks*

Stellar bars redistribute angular momentum in disk galaxies, driving their dynamical and secular evolution (Erwin et al. 2003; Kormendy & Kennicutt 2004; Jogee et al. 2004, 2005; Erwin 2005). Many barred galaxies host molecular gas concentrations of up to several thousand $M_\odot$ pc^{-2} in the inner kiloparsec, intense circumnuclear starburst rings, and disky bulges (e.g., Jogee 1999; Jogee et al. 2005). Bars are abundant in the field out to $z \sim 1.0$, corresponding to the last 8 Gyr (Elmegreen et al. 2004; Jogee et al. 2004; Zheng et al. 2005); however, we know much less about barred disks in dense clusters. Varela et al. (2004) note that bars are twice as frequent in perturbed galaxies as in isolated galaxies, and Elmegreen et al. (1990) note a higher frequency of bars in binary galaxy systems compared with isolated galaxies, so there is some evidence for variation with environment. The closest to a systematic environmental survey is that of van den Bergh (2002), who found the frequency of bars in spiral galaxies in clusters and in the field to be similar, although he did not probe the richest cluster environments.

Bars and similar structures (e.g., nuclear bars, rings, and spirals) are detectable in *HST* images if they have diameters ~3–5 FWHM (Sheth et al. 2003; Jogee et al. 2004; Lisker et al. 2006). At the resolution of the Coma survey they will be detected down to sizes of $r \sim 150$ pc. This will enable identification and characterization of unobscured large-scale bars across the Hubble sequence (e.g., Erwin 2005) and across different environments. In moderately inclined galaxies, the survey can identify compact disks and disky "pseudobulges" (Erwin et al. 2003; Kormendy & Kennicutt 2004; Athanassoula 2005; Jogee et al. 2005). Coma is an excellent case study for the significance of inner/nuclear components in S0 and spiral galaxies, and a key reference for comparison with studies of nuclear bar and ring frequencies in local field samples (e.g., Erwin & Sparke 2002; Laine et al. 2002; Knapen 2005).

The surface brightness profiles of stellar disks fall into three classes (Erwin et al. 2005, 2008; Pohlen & Trujillo 2006): classic single-exponential profiles, downward-bending "type II" profiles (Freeman 1970; "truncations"), and upward-bending "type III" profiles ("antitruncations"). Type II profiles are common in early-type barred galaxies and appear linked to the outer Lindblad resonance of bars; type III profiles, on the other hand, appear anticorrelated with bars and may be a signature of minor mergers (Younger et al. 2007). A comparison of barred S0–Sb galaxies

in the Virgo Cluster and the local field shows a dramatic dichotomy: type II profiles are common in the field but essentially absent in Virgo (Erwin et al. 2008). If this can be confirmed for the Coma Cluster, it points to a clear role for the cluster environment in shaping the outer disks of S0's and early-type spirals and suggests an important test for distinguishing models of S0 formation in clusters from the field.

2.4. *Color Gradients and Stellar Populations*

The steepness of the radial color gradients of dwarf and giant galaxies directly reflects their merging history: monolithic collapse imposes an initially steep negative metallicity gradient (Carlberg 1984), which will be progressively diluted by subsequent major mergers (Bekki & Shioya 1999; Kobayashi 2004). Semianalytic models of hierarchical galaxy formation predict differences in the merger history as a function of galaxy mass and environment (Cole et al. 2000). The Coma survey provides an unbiased sample of cluster dwarfs, so that the global scaling relations of different dwarf subtypes (dE, dS0, dE–N, dIrr) can be reliably determined. Coma elliptical galaxies have metallicities that seem to correlate with galaxy mass, which is broadly consistent with monolithic collapse models (e.g., Forbes et al. 2005). In contrast, dwarf elliptical and spheroidal galaxies display a variety of color gradients, even positive in some places, which is an indication of recent star formation (van Zee et al. 2004).

Complemented by *K*-band and integral field unit observations, the ACS images can be used to interpret the observed color distributions in terms of ages and metallicities, using photometric techniques (James et al. 2006) and line indices (e.g., Poggianti et al. 2001; Mehlert et al. 2003; Sánchez-Blázquez et al. 2006).

2.5. *Globular Clusters and Ultracompact Dwarfs*

The Coma Cluster hosts several bright early-type galaxies, which are known to have very rich globular cluster (GC) systems (Ashman & Zepf 1998), and many less massive galaxies with their own star cluster systems that were assembled and evolved in the dense Coma Cluster environment. There have been *HST* WFPC2 studies of the GC systems of a small number of bright Coma elliptical galaxies: IC 4051 (Baum et al. 1997; Woodworth & Harris 2000), NGC 4881 (Baum et al. 1995), and the cD galaxy NGC 4874 (Kavelaars et al. 2000; Harris et al. 2000). Marín-Franch & Aparicio (2002) find a wide range of specific frequency S_N values among the brighter galaxies in Coma, using the surface brightness fluctuation technique on ground-based data.

The ACS Virgo cluster survey has provided a number of important new results on the GC populations of early-type galaxies in the sparser Virgo Cluster (e.g., Jordán et al. 2005; Peng et al. 2006a; Mieske et al. 2006). At the distance of Coma it is only possible to resolve half-light radii down to $\sim$20 pc ($0.04''$). Moreover, the peak of the globular cluster luminosity function (GCLF) in Coma is suspected to be at $V = 27.88 \pm 0.12$ (Kavelaars et al. 2000), some 1.3 mag fainter than our 10 σ photometric completeness limit for point sources. Nevertheless, if the GCLF has a Gaussian form with $\sigma = 1.4$ mag, some 18% of the GCs are expected to be brighter than this limit, allowing us to study the color distributions, color-magnitude diagrams, and spatial distribution of GCs in a much wider range of galaxies than in the targeted Virgo Cluster survey (from $M_V = -23.3$ to -15), to a larger physical radius from the galaxy centers (up to 100 kpc). Stacking the GC systems of galaxies in bins will allow study of their properties as a function of host galaxy type, luminosity, and environment, and thus of the relationship between GC systems and their hosts, and the processes that lead to the formation of the rich GC systems of the massive galaxies (Pipino et al. 2007)

2.5.1. *The Spatial Distribution of Clusters and the Epoch of Reionization*

The old, metal-poor GC population in giant elliptical galaxies may provide the best available tracer of their dark halos and thus may be useful in testing the predictions of ΛCDM models. Moore et al. (2006) and Bekki & Yahagi (2006) find that the final radial distribution of the old GCs depends on the redshift of truncation of GC formation, which in turn might depend on the epoch of reionization. If the truncation is earlier, then the final radial GC distributions will be steeper and more compact (Bekki & Yahagi 2006).

Bassino et al. (2006) present a study of the globular clusters around NGC 1399, the dominant galaxy in the Fornax Cluster. They note a good agreement with a projected dark matter NFW (Navarro et al. 1996) density profile. Abadi et al. (2006) test the radial density profile of GCs around the somewhat isolated galaxies M31 and the Milky Way, comparing with the numerical simulations. They report that such luminous halos are similar in shape to their dark matter counterparts. On the other hand, Merritt et al. (2006), in a careful analysis of a set of ΛCDM simulations, find that the halo density distributions are better fit by the much earlier model of Einasto (1965, 1972, 1974) than by NFW or a number of other alternative models.

2.5.2. *Ultracompact Dwarfs and Transition Objects*

Ultracompact dwarfs (UCDs), at $-13.5 \leq M_V \leq -11.5$, have been detected from the ground in the Fornax and Virgo Clusters (Hilker et al. 1999; Drinkwater et al. 2000; Phillipps et al. 2001; Jones et al. 2006). *HST* imaging of the bright Fornax UCDs shows that they have half-light radii of 10–20 pc, larger than both Local Group GCs and typical dwarf galaxy nuclei but smaller than any previously known dwarf galaxies (De Propris et al. 2005). Similar but fainter objects have since been found (Haşegan et al. 2005; their dwarf galaxy globular cluster transition objects [DGTOs]). These overlap in luminosity with the brightest GCs, leading to the question of whether UCDs and large GCs are indeed fundamentally different objects. UCDs and DGTOs appear to be a feature of denser environments, so it is important to quantify the population of this new type of object in Coma and compare it with the less rich Virgo and Fornax.

Proposed scenarios see UCDs (see Hilker 2008 for a review) as the tidally "threshed" remnant nuclei of former nucleated dwarf elliptical galaxies in the cluster core (Bekki et al. 2001), the similar remains of late-type spirals with nuclear star clusters (Moore et al. 1998), more massive, perhaps intracluster versions of ordinary GCs (Hilker et al. 2004), merged (super)star clusters (Fellhauer & Kroupa 2002), products of massive starbursts during the merger of two gas-rich galaxies (Fellhauer & Kroupa 2005), or even leftover primordial building blocks of central galaxies in the dense galaxy cluster environment (Rakos & Schombert 2004).

The point-source magnitude limit of the Coma survey is deep enough to observe compact objects down to $M_V \simeq -9$ mag, so we can detect both UCDs and DGTOs down to GC luminosities. At the distance of Coma, the half-light radii of the brighter examples will be $0.02''$–$0.04''$, corresponding to $\sim$10–20 pc (Drinkwater et al. 2003). These sizes are similar to those of extended star clusters in the Virgo Cluster that have been successfully differentiated from point sources by Peng et al. (2006b) using ACS. They can be reliably distinguished from background galaxies at magnitudes

$V \sim 22$–25 mag, which have half-light radii typically between $0.2''$ and $1.0''$ (e.g., Roche et al. 1997).

2.6. *The Nature of "E+A" Galaxies*

Spectroscopic surveys (Caldwell et al. 1993; Poggianti et al. 2004) have identified several galaxies with poststarburst spectra in both the core and the infall region of Coma. Suggestions as to what triggered these bursts range from equal-mass galaxy mergers (Barnes & Hernquist 1992) to high-speed impact with shock fronts of infalling substructures (Poggianti et al. 2004) or generally with the dense ICM (Tran et al. 2005). The key to distinguishing between these processes is the spatial distribution of the intermediate-age populations. It would be concentrated to the center if major mergers were involved (Barnes & Hernquist 1992), while it would be either an extended or off-centered phenomenon if the galaxy had experienced an interaction with the ICM. The Coma survey includes a number of "E+A" or "k+a" galaxies at a range of luminosity, and the morphological features and color maps generated from the two ACS passbands will provide a valuable diagnostic of the physical origin of the E+A phenomenon.

2.7. *Nuclear Star Clusters and Central Massive Black Holes*

Massive black holes at the centers of spheroidal stellar systems correlate with the large-scale properties of the host spheroid. Popular correlations involve (1) spheroid velocity dispersion (Ferrarese & Merritt 2000; Gebhardt et al. 2000), (2) stellar concentration (Graham et al. 2001; Graham & Driver 2007), (3) luminosity (McLure & Dunlop 2002; Marconi & Hunt 2003; Graham 2007), and (4) mass (Marconi & Hunt 2003; Häring & Rix 2004).

The relationship between nuclear star clusters and central massive black holes is of increasing interest, although the formation of both remains poorly understood. Nuclear star clusters are observed in about 80% of intermediate-luminosity, early-type galaxies (e.g., Ferguson & Binggeli 1994; Graham & Guzmán 2003; Coté et al. 2006; Jordán et al. 2007; Balcells et al. 2007). Graham & Guzmán (2003) find that the luminosity of nuclear star clusters in dE's correlates strongly with the luminosity of the host spheroid. This luminosity trend has also been shown to exist in the bulges of lenticular and early-type spiral galaxies (Balcells et al. 2003). It has also been proposed that they follow the same $M_{\rm nucleus}$-$M_{\rm spheroid}$ relation as defined by supermassive black holes (Ferrarese et al. 2006b; Balcells et al. 2007), and the same $M_{\rm nucleus}$–Sérsic index relation (Graham & Driver 2007).

Graham & Driver (2007) suggest that the driving physical relation may be with the central stellar density (prior to core depletion) rather than a *global* property of the host spheroid. Given the known trend between central stellar density and host spheroid luminosity (e.g., Graham & Guzmán 2003; Merritt 2006a), the relations with global properties may be secondary in nature. It is therefore important to examine the connection between the mass of the nuclear star clusters and the central stellar density (projected, μ_0, and deprojected, ρ_0) of the host spheroid.

Study of the luminosity function, color-magnitude relation, relationship between nuclear and host galaxy color, and the radial distribution within the cluster (Ferguson & Sandage 1989; Lisker et al. 2007), and comparison with the lower density Fornax and Virgo environments, may help shed some light on potential formation mechanisms. Measurement of spatial offsets between nuclear clusters and the outer isophotes of the host galaxy may reveal an oscillation of the nucleus about the center of the potential, which will be of larger amplitude in shallower potentials (Binggeli et al. 2000). Furthermore, apparent double nuclei may in some cases be a sign of an edge-on nuclear disk (Kormendy 1988; Tremaine 1995), from which we may be able to determine the presence of a central massive black hole (e.g., Debattista et al. 2006).

Giant elliptical galaxies display cores that are partially depleted of stars. A possible mechanism is the slingshot action of supermassive black holes (SMBHs) from the progenitor galaxies as they sink to the center of the newly formed galaxy during a merger (Begelman et al. 1980; Ebisuzaki et al. 1991; Merritt et al. 2007). Cores may also be enlarged when black holes are ejected from galaxy centers by the gravitational wave rocket effect following coalescence of a SMBH binary (Redmount & Rees 1989; Merritt et al. 2004; Gualandris & Merritt 2008).

Using the core-Sérsic model (Graham et al. 2003a; Trujillo et al. 2004) it is possible to quantify the sizes (and mass deficits, $M_{\rm def}$) of these cores and to predict each galaxy's central black hole mass, $M_{\rm bh}$, using the measured Sérsic index n (e.g., Graham & Driver 2007). Given that $M_{\rm def}/M_{\rm bh}$ scales roughly linearly with N, where N is the number of major dry mergers, such measurements can be used to place constraints on the dry merger history of such cluster galaxies (Graham 2004; Ferrarese et al. 2006a; Merritt 2006b) and to constrain N as a function of galaxy magnitude.

3. SURVEY DESIGN

3.1. *Survey Area*

The ACS Wide Field Camera (WFC) has a field of view of 11.3 arcmin^2. The camera contains two 4096×2048 pixel CCDs, with an interchip gap of some $3''$. The capabilities of ACS at the time of our preanomaly observations are described in some detail by Pavlovsky et al. (2006).

The aim of the survey is to provide a large sample of galaxies for study in a high-density environment, and at the same time a comparison sample in a lower density region of the cluster for the specific science goals of examining the effect of environment on morphology, structural parameters, and stellar populations. Because of the density of confirmed cluster galaxies in the core (e.g., Colless & Dunn 1996), we have adopted a tiling strategy in the core region, tiling a region of approximately $18' \times 21'$, using 42 ACS pointings in a 7×6 pattern, with some overlap between adjacent tiles. An *HST* orientation of 282° was chosen for these tiles in order to maximize the time for which the obeservations could be scheduled in two-gyro mode (Sembach et al. 2006). A tile of the central mosaic was moved to the southern edge of the mosaic area, away from the star HD 112877 ($V = 7.17$), which would have a negative affect on ACS observations near its position.

In the outer part of the cluster the density of known members is less than one per ACS tile, and we decided to target known members that can be used to address some of our primary science goals. The best-studied region outside the core is the infall region around NGC 4839 (Neumann et al. 2001), where there have been a number of photometric surveys (Komiyama et al. 2002) and spectroscopic surveys for poststarburst galaxies (Caldwell et al. 1993), and line strengths and velocity dispersions of dwarf spheroidal galaxies (Poggianti et al. 2001; Matković & Guzmán 2005; A. Matković & R. Guzmán 2008, in preparation; Cody et al. 2007). Forty further ACS pointings were defined, each containing one, or in most cases more, cluster members from these spectroscopic surveys. In some cases the orientation was left free in the *HST* Phase 2 submission; in others a range was defined in order to ensure that more than one target galaxy was included. Table 2 lists the positions and orientations of our survey tiles. In this table column (1) gives the *HST* visit number within the program, and column (2), the field title. Columns (3) and (4) give the field center right ascension and declination,

TABLE 2

List of Survey Fields

Visit (1)	Field (2)	R.A. (J2000.0) (3)	Decl. (J2000.0) (4)	Orient (5)	Members (6)	Date of Observation (7)	Dither Positions Obtained (8)
1.....	Coma1_1	13 00 45.90	28 04 54.0	282.0	GMP 2440, GMP 2449, GMP 2489	2007 Jan 09	4
2.....	Coma1_2	13 00 30.30	28 04 54.0	282.0	GMP 2626, GMP 2559	2007 Jan 09	4
3.....	Coma1_3	13 00 14.70	28 04 54.0	282.0	GMP 2752, GMP 2787, GMP 2805, GMP 2784, GMP 2848, GMP 2861, GMP 2879, GMP 2922	2007 Jan 20	2
4.....	Coma1_4	12 59 59.10	28 04 54.0	282	GMP 3058	...	...
5.....	Coma1_5	12 59 43.50	28 04 54.0	282	GMP 3113, GMP 3121, GMP 3160	...	...
6.....	Coma7_6	12 59 06.30	27 45 48.0	282	GMP 3660, GMP 3730, GMP 3739, GMP 3750	...	...
7.....	Coma1_7	12 59 12.30	28 04 54.0	282	GMP 3561, GMP 3554, GMP 3656	...	...
8.....	Coma2_1	13 00 42.30	28 01 43.0	282.0	GMP 2417, GMP 2423, GMP 2511, GMP 2529, GMP 2551, GMP 2550, GMP 2559	2007 Jan 12	4
9.....	Coma2_2	13 00 26.70	28 01 43.0	282.0	GMP 2676, GMP 2727, GMP 2777	2007 Jan 13	4
10.....	Coma2_3	13 00 11.10	28 01 43.0	282.0	GMP 2839, GMP 2856, GMP 2940, GMP 2960	2007 Jan 13	4
11.....	Coma2_4	12 59 55.50	28 01 43.0	282	GMP 3073	...	...
12.....	Coma2_5	12 59 39.90	28 01 43.0	282.0	GMP 3312	2007 Jan 12	3
13.....	Coma2_6	12 59 24.30	28 01 43.0	282.0	GMP 3390, GMP 3406, GMP 3433, GMP 3438, GMP 3471	2007 Jan 13	2
14.....	Coma2_7	12 59 08.70	28 01 43.0	282.0	GMP 3681, GMP 3707, GMP 3762, GMP 3780, GMP 3811	2007 Jan 08	3
15.....	Coma3_1	13 00 38.70	27 58 32.0	282.0	GMP 2510, GMP 2516, GMP 2535	2007 Jan 26	4
16.....	Coma3_2	13 00 23.10	27 58 32.0	282.0	GMP 2651, GMP 2654, GMP 2718, GMP 2799, GMP 2815, GMP 2794, GMP 2798	2007 Jan 25	4
17.....	Coma3_3	13 00 07.50	27 58 32.0	282	GMP 2929, GMP 2921, GMP 2946, GMP 2964, GMP 2965, GMP 2985, GMP 2940	...	...
18.....	Coma3_4	12 59 51.90	27 58 32.0	282.0	GMP 3018, GMP 3098, GMP 3146, GMP 3166, GMP 3170, GMP 3206	2007 Jan 25	4
19.....	Coma3_5	12 59 36.30	27 58 32.0	282.0	GMP 3206, GMP 3213, GMP 3254, GMP 3269, GMP 3291, GMP 3292, GMP 3308, GMP 3329, GMP 3367, GMP 3414	2007 Jan 25	4
20.....	Coma3_6	12 59 20.70	27 58 32.0	282	GMP 3471, GMP 3484, GMP 3487, GMP 3489, GMP 3515, GMP 3534, GMP 3565, GMP 3602, GMP 3615, GMP 3639	...	...
21.....	Coma3_7	12 59 05.10	27 58 32.0	282	GMP 3664, GMP 3761, GMP 3851, GMP 3877, GMP 3794	...	...
22.....	Coma4_1	13 00 35.10	27 55 21.0	282.0	GMP 2541, GMP 2563, GMP 2571, GMP 2585, GMP 2591	2007 Jan 22	4
23.....	Coma4_2	13 00 19.50	27 55 21.0	282.0	GMP 2692, GMP 2736, GMP 2780, GMP 2778	2007 Jan 27	4
24.....	Coma4_3	13 00 03.90	27 55 21.0	282.0	GMP 2931, GMP 3017, GMP 3034	2007 Jan 24	4
25.....	Coma4_4	12 59 48.30	27 55 21.0	282.0	GMP 3068, GMP 3080, GMP 3133, GMP 3131, GMP 3201, GMP 3215, GMP 3222	2007 Jan 24	4
26.....	Coma4_5	12 59 32.70	27 55 21.0	282	GMP 3296, K9992, GMP 3325, GMP 3340, GMP 3352, GMP 3376, GMP 3424	...	...
27.....	Coma4_6	12 59 17.10	27 55 21.0	282	GMP 3486, GMP 3510, GMP 3511, GMP 3522, GMP 3645	...	...
28.....	Coma4_7	12 59 01.50	27 55 21.0	282	GMP 3719, GMP 3782, GMP 3855	...	...
29.....	Coma5_1	13 00 31.50	27 52 10.0	282	GMP 2716	...	...
30.....	Coma5_2	13 00 15.90	27 52 10.0	282	GMP 2716, GMP 2753, GMP 2852, GMP 2897, GMP 2910, GMP 2913	...	...
31.....	Coma5_3	13 00 00.30	27 52 10.0	282	GMP 2910, GMP 3052	...	...
32.....	Coma5_4	12 59 44.70	27 52 10.0	282	GMP 3178, GMP 3196, GMP 3205	...	...
33.....	Coma5_5	12 59 29.10	27 52 10.0	282.0	GMP 3311, GMP 3339, GMP 3383, GMP 3400, GMP 3423, GMP 3473	2007 Jan 15	4
34.....	Coma5_6	12 59 13.50	27 52 10.0	282	GMP 3557, GMP 3645, GMP 3706, GMP 3719, GMP 3733	...	...
35.....	Coma5_7	12 58 57.90	27 52 10.0	282	GMP 3821, GMP 3911, GMP 3946	...	...
36.....	Coma6_1	13 00 27.90	27 48 59.0	282	GMP 2603	...	...
37.....	Coma6_2	13 00 12.30	27 48 59.0	282	GMP 2783, GMP 2800, GMP 2956	...	...
38.....	Coma6_3	12 59 56.70	27 48 59.0	282	GMP 3092, GMP 3122, GMP 3126	...	...
39.....	Coma6_4	12 59 41.10	27 48 59.0	282	GMP 3126, GMP 3313, GMP 3324	...	...
40.....	Coma6_5	12 59 25.50	27 48 59.0	282	GMP 3403, GMP 3411, GMP 3425	...	...
41.....	Coma6_6	12 59 09.90	27 48 59.0	282	...	...	...
42.....	Coma6_7	12 58 54.30	27 48 59.0	282	GMP 3895, GMP 3896, GMP 3898, GMP 3925, GMP 3943, GMP 3949, GMP 3997	...	...
43.....	Outskirts_1	12 57 56.90	27 28 55.0	239–241	GMP 4522, GMP 4597, GMP 4630	...	...

TABLE 2—*Continued*

Visit (1)	Field (2)	R.A. (J2000.0) (3)	Decl. (J2000.0) (4)	Orient (5)	Members (6)	Date of Observation (7)	Dither Positions Obtained (8)
44.....	Outskirts_2	12 58 01.70	27 25 48.0	265–270	GMP 4479, GMP 4535, GMP 4577, GMP 4568	...	...
45.....	Outskirts_3	12 58 21.58	27 27 40.7	318.0	GMP 4206, GMP 4330, GMP 4381	2006 Nov 21	4
46.....	Outskirts_4	12 58 34.00	27 22 58.8	280.0	GMP 4192, GMP 4215	2007 Jan 17	4
47.....	Outskirts_5	12 57 27.38	27 28 59.1	219–221	GMP 4792, GMP 4794, GMP 4928, GMP 4943, GMP 4956	...	...
48.....	Outskirts_6	12 58 00.50	27 22 23.7	238–290	GMP 4484, GMP 4545, GMP 4565, GMP 4578	...	...
49.....	Outskirts_7	12 57 42.52	27 26 37.6	280–323	GMP 4692, GMP 4712, GMP 4768	...	...
50.....	Outskirts_8	12 57 27.40	27 23 37.0	230–323	GMP 4910, GMP 4918	...	...
51.....	Outskirts_9	12 57 04.70	27 21 25.1	260–323	GMP 5076, GMP 5136	...	...
52.....	Outskirts_10	12 56 44.30	27 26 12.0	250–323	GMP 5250, GMP 5255, GMP 5296	...	...
53.....	Outskirts_11	12 57 55.25	27 13 55.7	Any	GMP 4591	...	...
54.....	Outskirts_12	12 56 37.81	27 33 08.4	215–255	GMP 5284, GMP 5320, GMP 5364	...	...
55.....	Outskirts_13	12 57 04.22	27 31 34.5	299.1	GMP 5102	2007 Jan 19	4
56.....	Outskirts_14	12 57 26.40	27 32 54.4	220–323	GMP 4852, GMP 4907, GMP 4937	...	...
57.....	Outskirts_15	12 58 02.08	27 33 54.0	250–260	GMP 4447, GMP 4469, GMP 4579	...	...
58.....	Outskirts_16	12 58 34.59	27 33 43.3	220–225	GMP 4117, GMP 4156, GMP 4255	...	...
59.....	Outskirts_17	12 58 31.15	27 11 58.5	270.05	GMP 4135, GMP 4259, GMP 4294	2007 Jan 16	4
60.....	Outskirts_18	12 58 15.55	27 05 15.1	Any	GMP 4383	...	...
61.....	Outskirts_19	12 58 48.72	28 00 52.8	265–323	GMP 3969, GMP 3973, GMP 4003	...	...
62.....	Outskirts_20	12 56 36.03	26 54 17.8	Any	GMP 5361	...	...
63.....	Outskirts_21	12 56 29.80	27 13 32.8	265.0	GMP 5335, GMP 5359, GMP 5365, GMP 5472	2007 Jan 21	4
64.....	Outskirts_22	12 57 56.51	27 02 16.4	Any	GMP 4582, GMP 4596	...	...
65.....	Outskirts_23	12 57 21.08	27 00 04.2	220–260	GMP 4961, GMP 4980, GMP 4947	...	...
66.....	Outskirts_24	12 57 08.88	27 05 47.8	200–290	GMP 5032, GMP 5097	...	...
67.....	Outskirts_25	12 56 37.84	27 02 49.3	230–250	GMP 5283, GMP 5293, GMP 5294, GMP 5395	...	...
68.....	Outskirts_26	12 57 14.03	27 15 14.7	Any	GMP 5012, GMP 5019	...	...
69.....	Outskirts_27	12 59 12.21	27 36 56.9	265	GMP 3585, GMP 3598, GMP 3696	...	...
70.....	Outskirts_28	12 57 21.38	27 37 42.1	240–250	GMP 4888, GMP 4905, GMP 4967, GMP 4987	...	...
71.....	Outskirts_29	12 56 29.63	27 42 27.2	250–295	GMP 5345, GMP 5362, GMP 5434	...	...
72.....	Outskirts_30	12 55 38.57	27 44 39.9	284–286	GMP 5850, GMP 5912	...	...
73.....	Outskirts_31	12 57 03.95	27 45 06.4	225–235	GMP 5096, GMP 5100	...	...
74.....	Outskirts_32	12 58 25.87	26 54 23.2	245–255	GMP 4183, GMP 4340	...	...
75.....	Coma7_7	12 58 47.75	27 46 12.7	280.0	GMP 3949, GMP 3958, GMP 4035, GMP 4060	2007 Jan 17	4
76.....	Outskirts_34	12 58 19.13	27 45 44.6	Any	GMP 4341, GMP 4364	...	...
77.....	Outskirts_35	12 58 03.52	27 40 57.8	Any	GMP 4502, GMP 4557	...	...
78.....	Outskirts_36	12 57 10.80	27 24 18.0	314.52	GMP 5038	2006 Nov 27	4
79.....	Outskirts_37	12 57 50.52	27 38 38.8	Any	GMP 4632	...	...
80.....	Outskirts_38	12 56 04.00	27 09 03.0	Any	GMP 5676	...	...
81.....	Outskirts_39	12 59 50.50	27 44 48.9	230	GMP 3071, GMP 3132, GMP 3176, GMP 3192, GMP 3195, GMP 3211	...	...
82.....	Outskirts_40	12 56 14.60	27 30 23.2	Any	GMP 5546	...	...

NOTE.—Units of right ascension are hours, minutes, and seconds, and units of declination are degrees, arcminutes, and arcseconds.

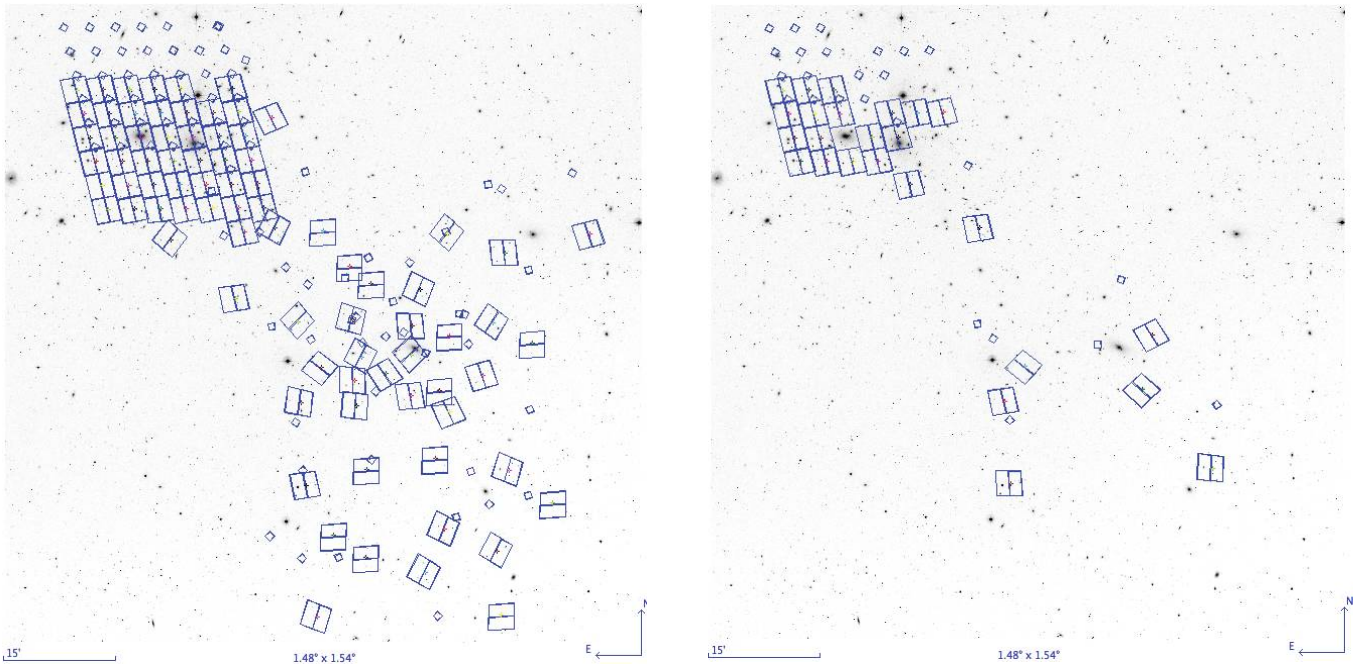

FIG. 2.—*Left:* Positions of ACS tiles for the survey proposed, overlaid on a DSS image of the core and infall region of the Coma Cluster. The small squares represent the fields of NICMOS parallel exposures. *Right:* Survey as at the ACS failure of 2007 January. Tiles shown have some or all of the proposed observations complete by this date. In this panel requested orientations are replaced by observed orientations if they differ.

respectively, and column (5), the field orientation of the observation, or the orientation specified for visits that have not yet been completed. Column (6) lists the spectroscopically confirmed cluster members within the field, with identifiers: GMP from Godwin et al. (1983); K from Komiyama et al. (2002). Column (7) gives the date of the observation, and column (8), the number of dither positions that have been observed by the time of the 2007 January ACS failure. At this time, 21 of our 82 fields have been fully observed, and a further four have either two or three dither positions observed. The survey is thus 28% complete.

Figure 2 (*left*) shows the positions and orientations of the survey tiles and the locations of NICMOS parallel observations. For cases where a range of orientations are specified in the Phase 2 submission the orientation shown is the midpoint of the range, and those tiles with free orientation are shown at 90°. The positions and final orientations of the 25 fully or partially observed fields are shown in the right- hand panel of this figure.

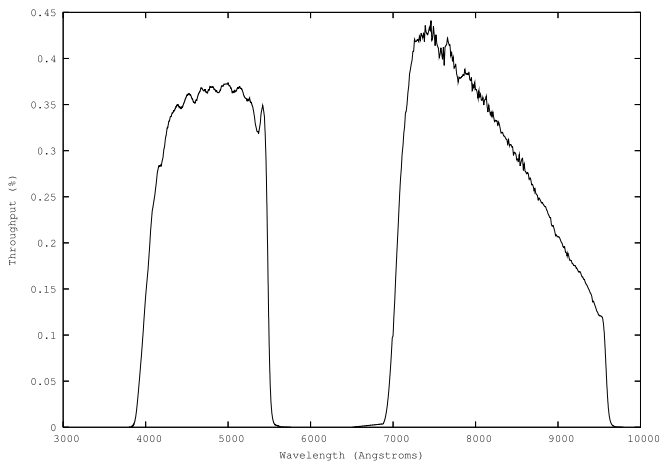

FIG. 3.—Total throughput curves of ACS CCDs plus filter for F475W passband (*left*) and F814W passband (*right*), after Sirianni et al. (2005).

3.2. *Choice of Passbands, Exposure Times, and Dither Parameters*

Color information is essential to some of the most important aims of the survey, so we require two passbands. For these passbands we choose F814W, as the passband that will give the deepest data for structural and luminosity function studies, and F475W, which is a compromise between color baseline and speed. These passbands are close to Cousins *I* and SDSS g', respectively. Transformations from these ACS WFC passbands to standard Johnson/Cousins passbands are given by Sirianni et al. (2005). Total system throughput as a function of wavelength for all ACS WFC filters, from the work of Sirianni et al. (2005), is given on the ACS project Web site,[30] and we plot in Figure 3 the throughput for our two passbands.

We defined a dithering pattern with a large (3″) dither across the inter-CCD gap on ACS WFC, plus a subdither to remove hot pixels, resulting in four positions over the two orbits. The large move was made between orbits. Each passband was observed at each dither position. The large dither point spacing was 3.011″ at a pattern orientation of 85.28°, and the hot pixel subdither spacing was 0.2412″ at a pattern orientation of 22.3239°. POS-TARG equivalent positions are given in Table 3.

[30] See http://adcam.pha.jhu.edu/instrument/photometry/.

TABLE 3
POS-TARG EQUIVALENT OF DITHER PATTERN USED

Dither Position	POS-TARG Position (arcsec)
1.....	(0.0, 0.0)
2.....	(0.222, 0.092)
3.....	(0.247, 3.001)
4.....	(0.469, 3.093)

TABLE 4
Point Source and Surface Brightness Detection Limits

Passband (1)	Exposure (s) (2)	ETC Limit (S/N = 10) "Default" (3)	ETC Limit (S/N = 10) "Optimal" (4)	Magnitude for 90% Recovery (5)	SB (mag arcsec^{-2}) S/N = 10 in 1 arcsec^2 (6)
F475W.....	2560	$g' = 26.75$	$g' = 27.6$	$g' = 27.55$	$g' = 25.8$
F814W.....	1400	$I_C = 25.95$	$I_C = 26.8$	$I_C = 26.65$	$I_C = 25.0$

Note.—Cols. (3) and (4): predicted 10 σ limits for optimal extraction of point sources; col. (5): limit for 90% recovery of injected point sources; col. (6): predicted surface brightness (1 arcsec^2) limits; all in the AB magnitude system.

Exposure times were 350 s in F814W and 640 s in F475W at each dither position. F814W frames are somewhat deeper than F475W, but it was not possible to distribute the time more toward F475W, as this would have resulted in F814W frames too short to dump the ACS buffer and thus a substantial increase in overheads. In some visits the F475W exposure time for the final dither position could be slightly longer, due to savings in the reacquisition overhead (as compared with the original acquisition), resulting in a total F475W integration time of between 2560 and 2680 s.

In Table 4 we present magnitudes and surface brightnesses for signal-to-noise ratio (S/N) = 10, calculated with the ACS Exposure Time Calculator (ETC). In these calculations the ETC is set to assume standard background conditions and an elliptical galaxy spectral energy distribution. The ETC gives two values for S/N for a point source: that in the "default" aperture, which for ACS WFC is a circle of 0.2″ radius; and an "optimal" S/N, assuming that a point-spread function (PSF) fitting algorithm is used. In columns (3) and (4) of Table 4 limits are presented in each passband for each of these S/N values to reach 10.

The real completeness and reliability limits, as well as the contamination with spurious sources near these magnitude limits, will depend on real background conditions, to which the halos of large galaxies will contribute, and on real *HST* guiding performance. For point sources we have estimated the limits by injecting artificial point sources into our ACS frames from one of our outer fields and recovering them with SExtractor. In column (5) of Table 4 we present the magnitude at which 90% of artificial injected sources are recovered. This limit is, as expected, between the two calculated limits, but encouragingly close to the "optimal S/N" calculated limits.

For galaxies the limits will depend on surface brightness and structural parameters. These will be discussed further in Paper II in this series (D. Hammer et al. 2008, in preparation).

In column (6) of Table 4 we present a calculated limit in mag arcsec^{-2}, obtained (using the ETC) for a S/N = 10 for a uniform surface brightness region of 1 arcsec^2. All magnitudes and surface brightnesses have been converted from the Vega magnitude system used by the ETC to AB magnitudes, using the AB magnitude of Vega in the chosen filters (e.g., Sirianni et al. 2005).

4. ACS DATA REDUCTION

The ACS data processing was performed at the Space Telescope Science Institute (STScI). It involved a dedicated pipeline based on a wrapper script using PyRAF/STSDAS modules that performed CCD data reduction and cosmic-ray cleaning, as well as the combination of individual dithered images using MultiDrizzle (Koekemoer et al. 2003), which makes use of the Drizzle software (Fruchter & Hook 2002) to remove geometric distortion and map the input exposures onto a rectified output frame. We describe details of the ACS data reduction below.

4.1. *Initial CCD Reduction*

As the observations of each *HST* visit were obtained, the data were run through the STScI on-the-fly-reprocessing (OTFR) pipeline for ACS data. This pipeline reduction involves basic CCD reduction by means of the IRAF/STSDAS task `calacs`, which performs bias subtraction, gain correction, dark subtraction, flat fielding, and the identification of bad pixels. Finally, the OTFR pipeline identifies the exposures taken through each filter (F475W vs. F814W) and combines them using the OTFR version of MultiDrizzle for ACS data. These first-pass pipeline products were used for quick-look purposes. Final images were created by a second-pass calibration procedure, which contained the steps described below.

4.2. *Updated Reference Files*

A few weeks after the each visit's data were observed, we downloaded more accurate calibration reference files from the *HST* archive, in particular the up-to-date superbias and superdark reference files, which were created from bias and dark exposures obtained contemporaneously with the science data (see, e.g., Lucas et al. 2006). These files were used for the final calibrations.

4.3. *Bias Level Offsets*

In virtually all ACS data sets of our Coma survey, we encountered significant bias level offsets between the four quadrants of the MultiDrizzle output images. These offsets, which ranged from a few tenths to several data numbers, are due to randomly varying differences between the bias level in the parallel overscan region of a given ACS WFC CCD chip and the level in its active region (see, e.g., Sirianni et al. 2003; note that ACS WFC contains four CCDs that are read out by their own amplifiers). A script was developed to measure these bias offsets between the four quadrants using iterative statistics on a large number of pairs of areas located close to (and symmetrically relative to) the quadrant-to-quadrant borders. The measured offsets were subtracted from the appropriate quadrants of the superbias reference file being used in the final image reduction of each set of exposures with a given filter.

4.4. *Image Registration*

In many cases, the spatial registration of images taken during each *HST* visit of this Coma treasury program was less accurate than expected, even though all images were planned to be taken without any change of prime guide star, telescope position, or roll angle. This problem was due to two compounding circumstances: (1) several visits were forced to use single-star guiding due to unforeseen problems with the *HST* Guide Star Catalog version 2 in the region of the Coma Cluster, and (2) the observations of our program unearthed a software bug in the ground system of the two-gyro guiding mode of *HST* for guide star reacquisitions when single guide stars were used. The result of

these issues was that significant spatial offsets are present between images (and their world coordinate system [WCS] header keywords) taken in different *HST* orbits, even if taken during one and the same visit. Since it is crucial to align images to better than ~5–8 mas (i.e., $\lesssim$0.15 ACS WFC pixel) in order to achieve accurate cosmic-ray rejection among the separate exposures within a visit and to retain satisfactory point-spread functions in the combined image, we registered all images within a visit to a common astrometric grid as follows.

First, we ran MultiDrizzle on every set of associated images (i.e., images taken in one visit with the same filter) using the `driz_separate = yes` setting. This created so-called singly drizzled images, which are the individual input science images in the same format as the default output files from MultiDrizzle, i.e., after correction for geometric distortion using the WCS keywords in the image header. SExtractor (Bertin & Arnouts 1996) was then run with a S/N threshold of S/N = 10 on each single drizzled image. The resulting catalogs were trimmed on the basis of object size and shape parameters, thereby rejecting the vast majority of cosmic rays, CCD artifacts, and diffuse extended objects. Further catalog trimming was done by visual inspection of the two-dimensional structure of the catalog sources, only retaining compact sources (nonsaturated stars and compact galaxies). Typically, 3–15 "good" sources remained available for proper image alignment. Using these object catalogs, residual shifts (called "delta shifts" in MultiDrizzle nomenclature) and rotations (Δx, Δy, $\Delta\theta$) between the individual singly drizzled images and a reference image were determined using IRAF tasks `xyxymatch` and `geomap`. The reference image was always taken to be the image observed first in the visit. The resulting delta shifts and rotations were then fed to a second run of MultiDrizzle using `driz_separate = yes` to verify the result of the alignment. This often prompted the need for a second iteration of the alignment process. The formal uncertainties of the alignment process stayed below 0.1 ACS WFC pixel (as reported by the `geomap` task).

4.5. *Cosmic-Ray Rejection*

Once the alignments between the individual images were determined, cosmic-ray rejection was done nominally in two steps. The first step was performed by using MultiDrizzle and its cosmic-ray rejection algorithm, which uses a process involving an image containing the median values of each pixel in the (geometrically corrected and aligned) input images, as well as its derivative (in which the value of each pixel represents the largest gradient from the value of that pixel to those of its direct neighbors; this image is used to avoid clipping bright point sources), to simulate a "clean" version of the final output image. For a typical 640 s F475W exposure, ~100,000–320,000 pixels were affected by cosmic-ray hits, i.e., ~0.6%–2% of the 4096^2 pixels. Thus, it is exceedingly rare for a pixel to be affected by cosmic rays during all four exposures (namely, $\leq$3 pixels out of 4096^2). The number of pixels affected by three cosmic rays out of four exposures was, however, significantly higher (up to ~120 pixels). In the latter cases, the median value was replaced by the value of the one valid pixel if the median value was larger than that of the valid pixel by a 5 σ threshold. This process yielded satisfactory results for the bulk of the tiles, except for the central strip of pixels in each tile, which only had contributions from two exposures due to the gap between the two CCD chips of ACS WFC. Furthermore, the MultiDrizzle output images of the tiles that only had two or three successful exposures also contained several residual pixels affected by cosmic rays. For the central strips in the tiles with four exposures and the full tiles with only two or three exposures, we therefore used a second step of cosmic-ray rejection by means of the `lacosmic` routine (van Dokkum 2001) using parameter values chosen after careful testing.

TABLE 5

NICMOS Parallel Observations—Field Centers and Exposures

Visit	R.A.	Decl.	Exposure per Filter (s)
1.....	13 00 53.82	28 13 10.9	2560
2.....	13 00 38.21	28 13 10.9	2560
3.....	13 00 22.61	28 13 11.0	1280
8.....	13 00 50.20	28 09 59.8	2560
9.....	13 00 34.61	28 09 59.9	2560
10.....	13 00 19.02	28 09 59.9	2560
12.....	12 59 47.81	28 09 59.8	1920
13.....	12 59 32.21	28 09 59.8	1280
14.....	12 59 16.61	28 09 59.9	1920
15.....	13 00 46.60	28 06 48.8	2560
16.....	13 00 31.01	28 06 48.9	2560
18.....	12 59 59.80	28 06 48.8	2560
19.....	12 59 44.21	28 06 49.9	2560
22.....	13 00 43.11	28 03 38.0	2560
23.....	13 00 27.40	28 03 38.0	2560
24.....	13 00 11.91	28 03 38.0	2560
25.....	12 59 56.31	28 03 38.0	2560
33.....	12 59 37.00	28 00 27.0	2560
45.....	12 58 49.90	27 33 21.2	2560
46.....	12 58 40.56	27 31 19.1	2560
55.....	12 57 22.73	27 38 58.6	2560
59.....	12 58 31.11	27 20 26.4	2560
63.....	12 56 26.40	27 21 58.4	2560
75.....	12 58 54.33	27 54 33.0	2560
78.....	12 57 37.50	27 30 20.6	2560

Note.—Units of right ascension are hours, minutes, and seconds, and units of declination are degrees, arcminutes, and arcseconds.

4.6. *Construction of Final ACS Images*

Before the final run of MultiDrizzle on the input images to produce the final image tiles using the cosmic-ray masks created as mentioned in the previous subsection, we created sky variance maps for each individual exposure for the purpose of deriving appropriate weight maps for the final image combination. These maps contain all components of noise in the images, except for the Poisson noise associated with the sources on the image. These maps were constructed from the sky values determined by MultiDrizzle for each individual exposure, the flat-field reference file, the dark current reference file, and the readout noise values as listed in the image headers for each individual image quadrant (or readout amplifier). These sky variance images were then inverted and used as weight maps for the associated exposures.

The final run of MultiDrizzle was performed by shrinking the input pixels by a factor of 0.8 at the stage when the PSF is convolved by the input pixel scale (i.e., the `final_pixfrac` parameter). This factor was arrived at after some experimentation with different values and was a good match to the degree of subsampling induced by the dither pattern that we used. The final output images were produced in the default unrotated frame of the ACS WFC CCDs rather than with north up so as to facilitate further analysis with PSF matching procedures.

5. NICMOS PARALLEL OBSERVATIONS

NICMOS parallel observations are made with the NIC3 camera of NICMOS in the *J* and *H* bands. The scientific motivations for these parallel observations, apart from that they are

TABLE 6
HST Data Products and Data Release Schedule

Data Product	Description	Release Date
Raw data	*HST* pipeline calibrated images	Immediate
Public catalog	Positions, magnitudes, geometry, color, from SExtractor	2008 May
Processed image data	Co-added, CR-cleaned, with best reference files	2008 May
Structural catalog	Multicomponent structural analysis	2008 Dec
External data	Redshifts and ground-based colors	2009 May

free, are the investigation of the near-IR luminosity function, to compare with the *Spitzer* LF of Jenkins et al. (2007); a study of intracluster GCs, where the combined ACS (g, I) and NICMOS (J, H) data can be used to separate intermediate-age GCs from old halo globular clusters (e.g., Puzia et al. 2002); and a study of the near-IR fundamental plane (FP) for dwarf galaxies, where the relative insensitivity of the IR luminosity to dust extinction reduces the scatter in the FP.

The NIC3 camera has a field of view of 51.2 arcsec^2; with the 3″ dither to accommodate the ACS inter-CCD gap, the uniformly exposed area is approximately $48'' \times 51''$ per visit. The NIC3 field center is some 8.5′ from the ACS field center, at a position angle that depends on the telescope orientation. The NICMOS fields are thus fairly random positions in the cluster, and as can be seen from Figure 2 only four of them overlap the area observed with ACS before the instrument failure. NICMOS parallel observations were taken on all pre-SM4 visits, of which 21 have the full four dither positions; these are summarized in Table 5. In 2560 s exposure per filter the calculated 10 σ magnitude limits for optimal extraction of point sources in the AB magnitude system are $J = 25.9$ and $H = 25.4$.

6. DATA AND EDUCATIONAL PRODUCTS

Data products will include image data as processed by the ACS pipeline described above, and also object catalogs with a variety of structural parameters as described in Paper II and subsequent papers in this series.

The calibrated ACS images produced by STScI have been ingested into Astro-WISE[31] (Valentijn et al. 2007; Valentijn & Verdoes Kleijn 2006). Astro-WISE connects the distributed research groups for the data analysis and is used to create the source catalogs for the ACS images and to model the surface brightness distributions of galaxies. The results will be publicly available via the Astro-WISE web services.

ACS data will be associated in Astro-WISE with all Coma Legacy Survey products including derived products and ancillary data (e.g., Subaru, INT, and UKIRT imaging and multiwavelength data). Astro-WISE also connects the survey to the EURO-VO.

Coma Legacy Survey data products will also be made available as part of the MAST Treasury archive at STScI.[32] Expected timescales for the distribution of data products are given in Table 6.

[31] See http://www.astro-wise.org/.
[32] See http://archive.stsci.edu/hst/tall.html.

An education and public outreach (EPO) program has been designed whose goal is to share the valuable legacy data set and the associated research with the public. The deliverables include:

1. *HST* ACS images of Coma that will appear at StarDate Online Astronomy Picture of the Week; in ViewSpace, which is seen in museums across the country; and in the revised StarDate/Universo Teacher Guide
2. An activity and DVD targeted at 9th–12th grade students; and revised Internet versions of the StarDate/Universo Teacher Guide, which will highlight research on the Coma Cluster from *HST* data
3. Five Stardate radio programs on the Coma Cluster in English, Spanish, and German for distribution on monthly compact disk to over 500 radio stations in the US, Mexico, and Germany

The EPO program is a coordinated effort between NASA, the University of Texas at Austin, the McDonald Observatory Education and Outreach Office, and the Space Telescope Science Institute (STScI).

This research and EPO program are supported by STScI through grants HST-GO-10861 and HST-E0-10861.35-A. We acknowledge Tony Roman and Marco Chiaberge at STScI for their technical help. D. C. acknowledges the support of STFC rolling grant PP/E001149/1, "Astrophysics Research at Liverpool John Moores University." S. J. acknowledges support from the National Aeronautics and Space Administration (NASA) LTSA grant NAG5-13063, and NSF grant AST 06-07748. A. W. G. is grateful for a Swinburne University of Technology RDS grant. T. H. P. gratefully acknowledges support in the form of a Plaskett Fellowship at the Herzberg Institute of Astrophysics. P. E. was supported by Deutsche Forschungsgemeinschaft Priority Program 1177. R. J. S. is supported under the STFC rolling grant PP/C501568/1 "Extragalactic Astronomy and Cosmology at Durham 2005–2010." R. G. acknowledges additional support from the NASA LTSA grant NAG5-11635. B. W. M. is supported by the Gemini Observatory, which is operated by the Association of Universities for Research in Astronomy, Inc., on behalf of the international Gemini partnership of Argentina, Australia, Brazil, Canada, Chile, the United Kingdom, and the United States of America. We thank the anonymous referee for very helpful comments.

REFERENCES

Abadi, M. G., Navarro, J. F., & Steinmetz, M. 2006, MNRAS, 365, 747
Adami, C., et al. 2006, A&A, 451, 1159
Adelman-McCarthy, J. K., et al. 2007, ApJS, 172, 634
Aguerri, J. A. L., Balcells, M., & Peletier, R. F. 2001, A&A, 367, 428
Aguerri, J. A. L., Iglesias-Páramo, J., Vílchez, J. M., Muñoz-Tuñón, C., & Sánchez-Janssen, R. 2005, AJ, 130, 475
Ashman, K. M., & Zepf, S. E. 1998, Globular Cluster Systems (Cambridge: Cambridge Univ. Press)
Athanassoula, E. 2005, MNRAS, 358, 1477
Babul, A., & Rees, M. J. 1992, MNRAS, 255, 346
Bai, L., Rieke, G. H., Rieke, M. J., Hinz, J. L., Kelly, D. M., & Blaylock, M. 2006, ApJ, 639, 827
Balcells, M., Graham, A. W., Domínguez-Palmero, L., & Peletier, R. F. 2003, ApJ, 582, L79
Balcells, M., Graham, A. W., & Peletier, R. F. 2007, ApJ, 665, 1084
Barnes, J., & Hernquist, L. 1992, ARA&A, 30, 705

Bassino, L. P., Faifer, F. R., Forte, J. C., Dirsch, B., Richtler, T., Geisler, D., & Schuberth, Y. 2006, A&A, 451, 789
Baum, W. A., Hammergren, M., Thomsen, B., Groth, E. J., Faber, S. M., Grillmair, C. J., & Ajhar, E. A. 1997, AJ, 113, 1483
Baum, W. A., et al. 1995, AJ, 110, 2537
Begelman, M. C., Blandford, R. D., & Rees, M. J. 1980, Nature, 287, 307
Bekki, K., Couch, W. J., & Drinkwater, M. 2001, ApJ, 552, L105
Bekki, K., & Shioya, Y. 1999, ApJ, 513, 108
Bekki, K., & Yahagi, H. 2006, MNRAS, 372, 1019
Bender, R., Burstein, D., & Faber, S. M. 1992, ApJ, 399, 462
Bernstein, G. M., Nichol, R. C., Tyson, J. A., Ulmer, M. P., & Wittman, D. 1995, AJ, 110, 1507
Bertin, E., & Arnouts, S. 1996, A&AS, 117, 393
Binggeli, B., Barazza, F., & Jerjen, H. 2000, A&A, 359, 447
Blanton, M. R., Lupton, R. H., Schlegel, D. J., Strauss, M. A., Brinkmann, J., Fukugita, M., & Loveday, J. 2005, ApJ, 631, 208
Bonamente, M., Joy, M. K., & Lieu, R. 2003, ApJ, 585, 722
Bothun, G. D., Schommer, R. A., & Sullivan, W. T. 1984, AJ, 89, 466
Bower, R. G., Lucey, J. R., & Ellis, R. S. 1992a, MNRAS, 254, 589
———. 1992b, MNRAS, 254, 601
Bowyer, S., Korpela, E. J., Lampton, M., & Jones, T. W. 2004, ApJ, 605, 168
Bravo-Alfuro, H., Cayatte, V., van Gorkom, J. H., & Balkowski, C. 2000, AJ, 119, 580
———. 2001, A&A, 379, 347
Briel, U. G., et al. 2001, A&A, 365, L60
Caldwell, N. 1983, AJ, 88, 804
Caldwell, N., Rose, J. A., Sharples, R. M., Ellis, R. S., & Bower, R. G. 1993, AJ, 106, 473
Caon, N., Capaccioli, M., & D'Onofrio, M. 1993, MNRAS, 265, 1013
Carlberg, R. G. 1984, ApJ, 286, 416
Cody, A. M., Carter, D., Bridges, T. J., Mobasher, B., & Poggianti, B. M. 2007, MNRAS, submitted
Cole, S., Lacey, C. G., Baugh, C. M., & Frenk, C. S. 2000, MNRAS, 319, 168
Colless, M., & Dunn, A. M. 1996, ApJ, 458, 435
Conselice, C. J., O'Neil, K., Gallagher, J. S., & Wyse, R. F. G. 2003, ApJ, 591, 167
Cooray, A., & Cen, R. 2005, ApJ, 633, L69
Coté, P., et al. 2006, ApJS, 165, 57
———. 2007, ApJ, 671, 1456
Debattista, V. P., Ferreras, I., Pasquali, A., Seth, A., De Rijcke, S., & Morelli, L. 2006, ApJ, 651, L97
De Propris, R., Phillipps, S., Drinkwater, M. J., Gregg, M. D., Jones, J. B., Evstigneeva, E., & Bekki, K. 2005, ApJ, 623, L105
Dressler, A. R. 1980, ApJ, 236, 351
Drinkwater, M. J., et al. 2000, Publ. Astron. Soc. Australia, 17, 227
———. 2003, Nature, 423, 519
Driver, S. P., Allen, P. D., Liske, J., & Graham, A. W. 2007a, ApJ, 657, L85
Driver, S. P., Couch, W. J., & Phillipps, S. 1998, MNRAS, 301, 369
Driver, S. P., Popescu, C. C., Tuffs, R., Graham, A. W., Liske, J., & Baldry, I. K. 2008, ApJ, in press
Driver, S. P., Popescu, C. C., Tuffs, R. J., Liske, J., Graham, A. W., Allen, P. D., & De Propris, R. 2007b, MNRAS, 379, 1022
Duc, P.-A., Bournard, F., & Masset, F. 2004, A&A, 427, 803
Ebisuzaki, T., Makino, J., & Okumura, S. K. 1991, Nature, 354, 212
Edwards, S. A., Colless, M., Bridges, T. J., Carter, D., Mobasher, B., & Poggianti, B. M. 2002, ApJ, 567, 178
Efstathiou, G. 2000, MNRAS, 317, 697
Einasto, J. 1965, Trudy Inst. Astrofiz. Alma-Ata, 5, 87
———. 1972, Galactic Models and Stellar Orbits (Tartu: Acad. Sci. Estonian SSR, Inst. Phys. Astron., W. Struve Astrophys. Obs)
———. 1974, in Proc. First European Astronomical Meeting, Stars and the Milky Way System, ed. L. N. Mavridis (Berlin: Springer), 291
Eisenhardt, P. R., De Propris, R., Gonzalez, A. H., Stanford, S. A., Wang, M., & Dickinson, M. 2007, ApJS, 169, 225
Elmegreen, B. G., Elmegreen, D. M., & Hirst, A. C. 2004, ApJ, 612, 191
Elmegreen, D. M., Elmegreen, B. G., & Bellin, A. D. 1990, ApJ, 364, 415
Erwin, P. 2005, MNRAS, 364, 283
Erwin, P., Beckman, J. E., & Pohlen, M. 2005, ApJ, 626, L81
Erwin, P., Pohlen, M., & Beckman, J. E. 2008, AJ, 135, 20
Erwin, P., Pohlen, M., Beckman, J. E., Gutierrez, L., & Aladro, R. 2008, in ASP Conf. Ser., Pathways through an Eclectic Universe, ed. J. H. Knapen, T. J. Mahoney, & A. Vazdekis (San Francisco: ASP), in press (arXiv: 0706.3829)
Erwin, P., & Sparke, L. S. 2002, AJ, 124, 65
Erwin, P., Vega Beltrán, J. C., Graham, A. W., & Beckman, J. E., & Pohlen, M. 2003, ApJ, 597, 929
Faber, S. M., & Jackson, R. E. 1976, ApJ, 204, 668
Fellhauer, M., & Kroupa, P. 2002, MNRAS, 330, 642
———. 2005, MNRAS, 359, 223
Ferguson, H., & Binggeli, B. 1994, A&A Rev., 6, 67
Ferguson, H., & Sandage, A. 1989, ApJ, 346, L53
Ferguson, H. C., & Sandage, A. R. 1991, AJ, 101, 765
Ferrarese, L., & Merritt, D. 2000, ApJ, 539, L9
Ferrarese, L., et al. 2006a, ApJS, 164, 334
———. 2006b, ApJ, 644, L21
Finoguenov, A., Briel, U. G., Henry, J. P., Gavazzi, G., Iglesias-Paramo, J., & Boselli, A. 2004, A&A, 419, 47
Forbes, D., Sánchez-Blázquez, P., & Proctor, R. 2005, MNRAS, 361, L6
Freeman, K. C. 1970, ApJ, 160, 811
Fruchter, A. S., & Hook, R. N. 2002, PASP, 114, 144
Gardner, J. P., Sharples, R. M., Frenk, C. S., & Carrasco, B. E. 1997, ApJ, 480, L99
Gavazzi, G., O'Neil, K., Boselli, A., & van Driel, W. 2006, A&A, 449, 929
Gebhardt, K., et al. 2000, AJ, 119, 1157
Geller, M. J., & Huchra, J. P. 1989, Science, 246, 897
Godwin, J. G., Metcalfe, N., & Peach, J. V. 1983, MNRAS, 202, 113
Godwin, J. G., & Peach, J. V. 1977, MNRAS, 181, 323
Graham, A. W. 2004, ApJ, 613, L33
———. 2007, MNRAS, 379, 711
Graham, A. W., & Driver, S. P. 2007, ApJ, 655, 77
Graham, A. W., Erwin, P., Caon, N., & Trujillo, I. 2001, ApJ, 563, L11
Graham, A. W., Erwin, P., Trujillo, I., & Asensio-Ramos, A. 2003a, AJ, 125, 2951
Graham, A. W., & Guzmán, R. 2003, AJ, 125, 2936
Graham, A. W., Jerjen, H., & Guzmán, R. 2003b, AJ, 126, 1787
Gregg, M. D. 1997, NewA, 1, 363
Gualandris, A., & Merritt, D. 2008, ApJ, 678, 780
Gutiérrez, C. M., Trujillo, I., Aguerri, J. A. L., Graham, A. W., & Caon, N. 2004, ApJ, 602, 664
Guzmán, R., Lucey, J. R., & Bower, R. G. 1993, MNRAS, 265, 731
Guzmán, R., Lucey, J. R., Carter, D., & Terlevich, R. J. 1992, MNRAS, 257, 187
Häring, N., & Rix, H.-W. 2004, ApJ, 604, L89
Harris, W. E., Kavelaars, J. J., Hanes, D. A., Hesser, J. E., & Pritchet, C. J. 2000, ApJ, 533, 137
Haşegan, M., et al. 2005, ApJ, 627, 203
Hilker, M. 2008, in Globular Clusters—Guides to Galaxies, ed. T. Richtler & S. Larsen (Berlin: Springer), in press (astro-ph/0605447)
Hilker, M., Infante, L., Vieira, G., Kissler-Patig, M., & Richtler, T. 1999, A&AS, 134, 75
Hilker, M., Kayser, A., Richtler, T., & Willemsen, P. 2004, A&A, 422, L9
Hjorth, J., & Tanvir, N. R. 1997, ApJ, 482, 68
Hornschemeier, A. E., Mobasher, B., Alexander, D. M., Bauer, F. E., Bautz, M. W., Hammer, D., & Poggianti, B. M. 2006, ApJ, 643, 144
James, P. A., Salaris, M., Davies, J. I., Phillipps, S., & Cassisi, S. 2006, MNRAS, 367, 339
Jenkins, L. P., Hornschemeier, A. E., Mobasher, B., Alexander, D. M., & Bauer, F. E. 2007, ApJ, 666, 846
Jensen, J. B., Tonry, J., & Luppino, G. 1999, ApJ, 510, 71
Jogee, S. 1999, Ph.D. thesis, Yale Univ.
Jogee, S., Scoville, N., & Kenney, J. D. P. 2005, ApJ, 630, 837
Jogee, S., et al. 2004, ApJ, 615, L105
Jones, J. B., et al. 2006, AJ, 131, 312
Jordán, A., et al. 2005, ApJ, 634, 1002
———. 2007, ApJS, 169, 213
Jorgensen, I. 1999, MNRAS, 306, 607
Jorgensen, I., Chiboucas, K., Flint, K., Bergmann, M., Barr, J., & Davies, R. L. 2006, ApJ, 639, L9
Jorgensen, I., Franx, M., & Kjaergaard, P. 1996, MNRAS, 280, 167
Kaastra, J. S., Lieu, R., Tamura, T., Paerels, F. B. S., & den Herder, J. W. 2003, A&A, 397, 445
Kavelaars, J. J., Harris, W. E., Hanes, D. A., Hesser, J. E., & Pritchet, C. J. 2000, ApJ, 533, 125
Knapen, J. H. 2005, A&A, 429, 141
Kobayashi, C. 2004, MNRAS, 347, 740
Kochanek, C. S., et al. 2001, ApJ, 560, 566
Koekemoer, A. M., Fruchter, A. S., Hook, R. N., & Hack, W. 2003, in 2002 *HST* Calibration Workshop, ed. S. Arribas, A. Koekemoer, & B. Whitmore (Baltimore: STScI), 337
Komiyama, Y., et al. 2002, ApJS, 138, 265
Kormendy, J. 1985, ApJ, 295, 73
———. 1988, ApJ, 325, 128
Kormendy, J., & Kennicutt, R. C., Jr. 2004, ARA&A, 42, 603
Laine, S., Shlosman, I., Knapen, J. H., & Peletier, R. F. 2002, ApJ, 567, 97
Laurikainen, E., Salo, H., & Buta, R. 2005, MNRAS, 362, 1319
Lieu, R., Mittaz, J. P. D., Bowyer, S., Breen, J. O., Lockman, F. J., Murphy, E. M., & Hwang, C.-Y. 1996, Science, 274, 1335

Lisker, T., Debattista, V. P., Ferreras, I., & Erwin, P. 2006, MNRAS, 370, 477
Lisker, T., Grebel, E. K., Bingelli, B., & Glatt, K. 2007, ApJ, 660, 1186
Lucas, R. A., Swam, M., Mutchler, M., & Sirianni, M. 2006, in 2005 *HST* Calibration Workshop, ed. A. Koekemoer, P. Goudfrooij, & L. Dressel (Baltimore: STScI), 61
Lucey, J. R., Guzmán, R., Carter, D., & Terlevich, R. J. 1991, MNRAS, 253, 584
Marconi, A., & Hunt, L. K. 2003, ApJ, 589, L21
Marín-Franch, A., & Aparicio, A. 2002, ApJ, 568, 174
Mastropietro, C., Moore, B., Mayer, L., Debattista, V. P., Piffaretti, R., & Stadel, J. 2005, MNRAS, 364, 607
Matković, A., & Guzmán, R. 2005, MNRAS, 362, 289
Matković, A., Guzmán, R., Sánchez-Blázquez, P., Gorgas, J., Cardiel, N., & Gruel, N. 2007, MNRAS, submitted
McLure, R. J., & Dunlop, J. S. 2002, MNRAS, 331, 795
Mehlert, D., Thomas, D., Saglia, R. P., Bender, R., & Wegner, G. 2003, A&A, 407, 423
———. 2006a, Rep. Prog. Phys., 69, 2513
———. 2006b, ApJ, 648, 976
Merritt, D., Graham, A. W., Moore, B., Diemand, J., & Terzic, B. 2006, AJ, 132, 2685
Merritt, D., Mikkola, S., & Szell, A. 2007, ApJ, 671, 53
Merritt, D., Milosavljević, M., Favata, M., Hughes, S. A., & Holz, D. E. 2004, ApJ, 607, L9
Mieske, S., Hilker, M., Infante, L., & Mendes de Oliveira, C. 2007, in Proc. IAU Symp. 244, Dark Galaxies and Lost Baryons, ed. J. I. Davies & M. J. Disney (Cambridge: Cambridge Univ. Press), 331
Mieske, S., et al. 2006, ApJ, 653, 193
Milne, M. L., Pritchet, C. J., Poole, G. B., Gwyn, S. D. J., Kavelaars, J. J., Harris, W. E., & Hanes, D. A. 2007, AJ, 133, 177
Mobasher, B., et al. 2001, ApJS, 137, 279
———. 2003, ApJ, 587, 605
Moore, B., Katz, N., Lake, G., Dressler, A., & Oemler, A. 1996, Nature, 379, 613
Moore, B., Lake, G., & Katz, N. 1998, ApJ, 495, 139
Moore, B., et al. 2006, MNRAS, 368, 563
Moore, S. A. W., Lucey, J. R., Kuntschner, H., & Colless, M. 2002, MNRAS, 336, 382
Navarro, J. F., Frenk, C. S., & White, S. D. M. 1996, ApJ, 462, 563
Nelan, J. E., et al. 2005, ApJ, 632, 137
Neumann, D. M., et al. 2001, A&A, 365, L74
Pavlovsky, C., et al. 2006, Advanced Camera for Surveys Instrument Handbook for Cycle 16, version 7.1 (Baltimore: STScI)
Peng, E. W., et al. 2006a, ApJ, 639, 95
———. 2006b, ApJ, 639, 838
Phillipps, S., Drinkwater, M. J., Gregg, M., & Jones, J. B. 2001, ApJ, 560, 201
Phillipps, S., Driver, S. P., Couch, W. J., & Smith, R. M. 1998, ApJ, 498, L119
Pipino, A., Puzia, T. H., & Matteucci, F. 2007, ApJ, 665, 295
Poggianti, B. M., et al. 2001, ApJ, 562, 689
———. 2004, ApJ, 601, 197
Pohlen, M., & Trujillo, I. 2006, A&A, 454, 759
Puzia, T. H., Zepf, S. E., Kissler-Patig, M., Hilker, M., Minniti, D., & Goudfrooij, P. 2002, A&A, 391, 453
Rakos, K., & Schombert, J. 2004, AJ, 127, 1502
Redmount, I. H., & Rees, M. J. 1989, Comments Astrophys., 14, 165
Renaud, M., Bélanger, G., Paul, J., Lebrun, F., & Terrier, R. 2006, A&A, 453, L5
Roberts, S., et al. 2004, MNRAS, 352, 478
Roche, N., Ratnatunga, K., Griffiths, R. E., & Im, M. 1997, MNRAS, 288, 200
Sabatini, S., Davies, J. I., Roberts, S., & Scaramella, R. 2007, in Proc. IAU Symp. 244, Dark Galaxies and Lost Baryons, ed. J. I. Davies & M. J. Disney (Cambridge: Cambridge Univ. Press), 311
Sánchez-Blázquez, P., Gorgas, J., & Cardiel, N. 2006, A&A, 457, 823
Sembach, K. R., et al. 2006, *HST* Two-Gyro Handbook, version 3.0 (Baltimore: STScI)
Sérsic, J. L. 1968, Atlas de Galaxias Australes (Córdoba: Obs Astron., Univ. Nac. Córdoba)
Sheth, K., Regan, M. W., Scoville, N. Z., & Strubbe, L. E. 2003, ApJ, 592, L13
Sirianni, M., Martel, A. R., Jee, M. J., Van Orsow, D., & Sparks, W. B. 2003, in 2002 *HST* Calibration Workshop, ed. S. Arribas, A. Koekemoer, & B. Whitmore (Baltimore: STScI), 82
Sirianni, M., et al. 2005, PASP, 117, 1049
Smith, R. J., Hudson, M. J., Lucey, J. R., Nelan, J. E., & Wegner, G. A. 2006, MNRAS, 369, 1419
Smith, R. J., et al. 2004, AJ, 128, 1558
Smith, R. M., Driver, S. P., & Phillipps, S. 1997, MNRAS, 287, 415
Somerville, R. S., & Primack, J. R. 1999, MNRAS, 310, 1087
Thomsen, B., Baum, W. A., Hammergren, M., & Worthey, G. 1997, ApJ, 483, L37
Tran, K.-V. H., van Dokkum, P., Illingworth, G. D., Kelson, D., Gonzalez, A., & Franx, M. 2005, ApJ, 619, 134
Tremaine, S. 1995, AJ, 110, 628
Trentham, N., & Hodgkin, S. 2002, MNRAS, 333, 423
Trentham, N., & Tully, R. B. 2002, MNRAS, 335, 712
Trentham, N., Tully, R. B., & Verheijen, M. A. W. 2001, MNRAS, 325, 385
Trujillo, I., Erwin, P., Asensio Ramos, A., & Graham, A. W. 2004, AJ, 127, 1917
Tully, R. B., & Pierce, M. J. 2000, ApJ, 533, 744
Tully, R. B., Somerville, R., Trentham, N., & Verheijen, M. A. W. 2002, ApJ, 569, 573
Valentijn, E. A., & Verdoes Kleijn, G. 2006, ERCIM News, 65, 20
Valentijn, E. A., et al. 2007, in ASP Conf. Ser. 376, Astronomical Data Analysis Software and Systems XVI, ed. R. A. Shaw, F. Hill, & D. J. Bell (San Francisco: ASP), 491
van den Bergh, S. 2002, AJ, 124, 782
van Dokkum, P. G. 2001, PASP, 113, 1420
van Zee, L., Barton, E., & Skillman, E. D. 2004, AJ, 128, 2797
Varela, J., Moles, M., Márquez, I., Galletta, G., Masegosa, J., & Bettoni, D. 2004, A&A, 420, 873
Vogt, N. P., Haynes, M. P., Herter, T., & Giovanelli, R. 2004, AJ, 127, 3273
White, S. D. M., Briel, U. G., & Henry, J. P. 1993, MNRAS, 261, L8
Wirth, A., & Gallagher, J. S. 1984, ApJ, 282, 85
Woodworth, S. C., & Harris, W. E. 2000, AJ, 119, 2699
Younger, J. D., Cox, T. J., Seth, A. C., & Hernquist, L. 2007, ApJ, 670, 269
Zheng, X. Z., Hammer, F., Flores, H., Assémat, F., & Rawat, A. 2005, A&A, 435, 507
Zwaan, M. A., Meyer, M. J., Stavely-Smith, L., & Webster, R. L. 2005, MNRAS, 359, L30